JCTC Journal of Chemical Theory and Computation

Article

pubs.acs.org/JCTC

Ab Initio Optoelectronic Properties of Silicon Nanoparticles: Excitation Energies, Sum Rules, and Tamm−Dancoff Approximation

Dario Rocca,*[,†,‡] Márton Vörös,[§,∥] Adam Gali,[∥,⊥] and Giulia Galli[#]

[†]Université de Lorraine, CRM[2], UMR 7036, Institut Jean Barriol, 54506 Vandoeuvre-lès-Nancy, France

[‡]CNRS, CRM[2], UMR 7036, 54506 Vandoeuvre-lès-Nancy, France

[§]Department of Physics, University of California, Davis, California 95616, United States

[∥]Department of Atomic Physics, Budapest University of Technology and Economics, Budafoki út 8, H-1111, Budapest, Hungary

[⊥]Institute for Solid State Physics and Optics, Wigner Research Center for Physics, Hungarian Academy of Sciences, P.O. Box 49, H-1525 Budapest, Hungary

[#]Institute for Molecular Engineering, The University of Chicago, Chicago, Illinois 60637, United States

ABSTRACT: We present an ab initio study of the excited state properties of silicon nanoparticles (NPs) with diameters of 1.2 and 1.6 nm. Quasiparticle corrections were computed within the G_0W_0 approximation. The absorption spectra were computed by time-dependent density functional theory (TDDFT) using the adiabatic PBE approximation, and by solving the Bethe−Salpeter equation (BSE). In our calculations, we used recently developed methods that avoid the explicit inversion of the dielectric matrix and summations over empty electronic states. We found that a scissor operator reliably describes quasiparticle corrections for states in the low energy part of the spectra. Our results also showed good agreement between the positions of the absorption peaks obtained using TDDFT and the BSE in the low part of the spectra, although the peak intensities differ. We discuss the effect of the Tamm−Dancoff approximation on the optical properties of the NPs and present a quantitative analysis in terms of sum rules. In the case of the BSE we found that, even in the absence of the Tamm−Dancoff approximation, the f-sum rule is not fully satisfied due to an inconsistency between the approximations used for the BSE kernel and for the quasiparticle Hamiltonian.

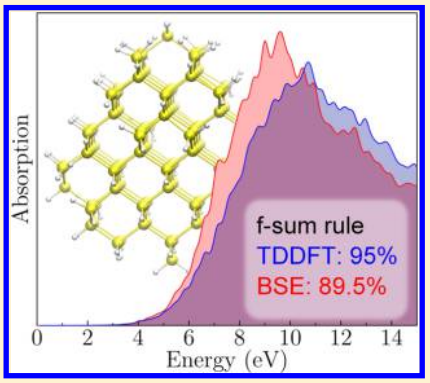

1. INTRODUCTION

The Bethe−Salpeter equation, based on the GW approximation, and time-dependent density functional theory are considered state-of-the-art methods to compute neutral electronic excitations in realistic materials.[1−11] In particular, the Bethe−Salpeter equation (BSE) has been shown to accurately describe the optical properties of several bulk solids[2,4,12−16] and extended nanostructures, such as nanotubes[17,18] and nanowires.[19,20] The performance of the BSE for electronic excitations of molecules and zero dimensional systems is not as well understood, and the shortcomings of widely used approximations, such as the Tamm-Dancoff approximation, have been pointed out for several finite systems.[21,22] On the contrary, time-dependent density functional theory (TDDFT) has been widely applied to describe molecular excitations, leading to accurate results in several instances.[9,23−25] However, TDDFT in the standard adiabatic approximations with local, or semilocal functionals has well-known shortcomings in the description of excitons in solids[15,26] and Rydberg and charge transfer excitations in molecules.[22,27−32] An improved formulation of TDDFT to describe optical absorption in solids was recently proposed by deriving a specific kernel from the BSE.[33,34] Within this framework, TDDFT yields results in agreement with those of BSE for several solids, but the computational cost is comparable to the solution of the full BSE.

Due to the approximations and numerical complexity involved in both the solution of the BSE and TDDFT, comparisons of results obtained with the two methods have long been challenging, especially for molecules and zero dimensional nanostructures. For example, the results of TDLDA (TDDFT using the adiabatic local density approximation (LDA)) and BSE calculations have been compared for a series of small hydrogenated silicon nanoparticles.[35−37] For the smaller nanoparticles (including silane SiH_4), TDLDA and BSE yield absorption spectra which differ both in the peak positions and intensities. For larger sizes, these two methods appear to produce results in better agreement with each other, although the detailed features and the onset of the spectra still differ.[35−37]

In this work, we present a comparison of the absorption spectra of Si nanoparticles of about 1 and 2 nm, obtained within TDDFT and by solving the BSE. We used newly developed techniques to compute GW corrections to Kohn−Sham eigenvalues[38,39] and to solve the BSE,[15,22] which allow for

Received: February 6, 2014
Published: May 27, 2014

 © 2014 American Chemical Society dx.doi.org/10.1021/ct5000956 | J. Chem. Theory Comput. 2014, 10, 3290−3298

calculations for systems with several hundreds of electrons.[11] We considered two hydrogenated silicon nanoparticles with diameters of 1.2 and 1.6 nm, with 130 and 220 atoms and 328 and 592 valence electrons, respectively. The size of these nanoparticles is considerably larger than those investigated in previous studies based on the BSE;[35−37] hence, this work represents a major computational effort[40] in applying sophisticated many-body perturbation theory techniques to nanostructures of sizes attainable experimentally.[41,42]

We show that for silicon nanoparticles of ≈1 to ≈2 nm diameter the absorption spectra obtained at the TDLDA and BSE levels of theory exhibit peaks located in similar positions (within 0.1−0.2 eV) in the low energy part of the spectra. However, the overall peak intensities differ. These differences are analyzed in detail, by investigating the validity of sum rules and the reliability of the Tamm−Dancoff approximation within the two levels of theory.

The rest of the paper is organized as follows. In section 2, we summarize the methods used to compute the GW/BSE and TDDFT spectra for systems with several hundreds of valence electrons, including computational details. In section 3, we present the computed optical absorption spectra for the $Si_{66}H_{64}$ and the $Si_{124}H_{96}$ nanoparticles and discuss the comparison of TDDFT and BSE results. In section 4, we discuss the effect of the Tamm−Dancoff approximation on the computed spectra and the comparison of the two methods. Section 5 presents our conclusions.

2. METHOD

We performed GW calculations starting from density functional theory (DFT) single particle energies and orbitals obtained within the generalized gradient approximation PBE.[43] The non-self-consistent perturbative GW approach is often denoted as G_0W_0 method. For the sake of simplicity in this paper GW will be used to indicate the perturbative G_0W_0 approach.

We used the GW implementation presented in refs 38 and 39, which is based on plane-wave basis set and pseudopotentials, and modules of the Quantum Espresso package.[44] Within this approach, the dielectric matrix ε is efficiently represented through a spectral decomposition.[11,45,46] The lowest eigenvalues and eigenvectors (eigenpotentials) of the dielectric matrix are obtained by an iterative procedure based on density functional perturbation theory (DFPT),[47] which does not require the explicit calculation of the conduction (or virtual) states of the ground-state Hamiltonian. The dynamical effects in the dielectric matrix and in the Green's function are then included by using the Lanczos algorithm.[38,48,49] Within this framework the accuracy is controlled by a single parameter, the number of eigenvectors of ε, and the slow convergence of GW quasiparticle energies with respect to the number of conduction states and the energy cutoff used to represent ε is avoided.

The BSE calculations were performed by using the density matrix perturbation theory formulation presented in refs 11, 15, 20, and 22. Within this formalism the quantum-Liouville equation including a static self-energy operator is linearized with respect to an external perturbation. The perturbed density matrix is then represented using a projector onto the conduction state subspace, thus avoiding the calculation of conduction states of the ground state Hamiltonian. Similar to the GW method described above, the dielectric matrix necessary to compute the BSE kernel is obtained by iterative diagonalization.[45] In order to obtain a straightforward comparison between BSE and TDDFT, the TDDFT calculations were carried out with the turboTDDFT code, which uses a framework similar to the one described above for the BSE.[48,50,51] The main equations used in our BSE implementation are summarized in Appendix A, where the validity of sum rules for the BSE is also discussed.

Two nanoparticles were considered in our calculations: $Si_{66}H_{64}$ and $Si_{124}H_{96}$, corresponding to diameters of 1.2 and 1.6 nm, respectively (the diameter is defined as the maximum Si−Si distance). The initial geometries of the nanoparticles were generated by cutting out a spherical portion of bulk silicon and then by saturating the resulting dangling bonds with hydrogen atoms. Their geometry was then relaxed until the forces were smaller than 10^{-5} Ry/Bohr, using a plane wave energy cutoff of 35 Ry.

For the excited state calculations a cutoff of 25 Ry was used for both nanoparticles. In order to simulate isolated nanoparticles in a periodic cell and avoid spurious interactions between periodic replica, a 53^3 $Bohr^3$ supercells were used for $Si_{66}H_{64}$ and $Si_{124}H_{96}$. We used pseudopotentials from the Quantum Espresso library[44] and the PBE functional.[43] The BSE and TDDFT absorption coefficients $I(\omega)$ were computed as the imaginary part of $\omega \mathrm{Tr}(\alpha(\omega))$, where ω is the energy of the incident photons, α is the dynamical polarizability, and Tr indicates the trace operator.[22,48,50] A Lorentzian broadening of 0.08 eV was added to the computed spectra. We used 600 eigenvalues and eigenvectors (N_{eig}) in the spectral decomposition of the dielectric matrix. We note that the eigenvalues λ_i of the dielectric matrix are ≥ 1 and $(\lambda_i - 1)$ goes rapidly to 0 as a function of i; hence, only a relatively small number N_{eig} (approximately equal to the number of electrons in the system) is sufficient to accurately represent the dielectric matrix.[45] This number is much smaller than the number of pairs $\phi_c\phi_v$ (where c and v denote virtual and occupied states, respectively) that one would need if straightforward summations on virtual states were carried out.[52] In the GW calculations, where in several cases convergence with respect to N_{eig} was found to be slower than for the solution of the BSE, the accuracy of our results was checked by considering up to 840 eigenpotentials. In the case of $Si_{66}H_{64}$ the value of the gap decreased by 0.047 eV by increasing the number of eigenpotentials form 600 to 840, while for $Si_{124}H_{96}$ the gap decreased by 0.052 eV.

3. OPTICAL PROPERTIES OF HYDROGENATED SILICON NANOPARTICLES

The computed gap of $Si_{66}H_{64}$ is 2.92 and 5.55 eV (obtained with 840 eigenpotentials) at the PBE and GW levels of theory, respectively. We computed GW quasiparticle energies for several states close to the HOMO and LUMO levels, from state 100 to state 300 (this system has 164 doubly occupied states). The difference $[\varepsilon^{GW}-\varepsilon^{PBE}]$ between the GW and PBE energies as a function of the eigenvalue index is shown in Figure 1.[53] The large jump in $[\varepsilon^{GW}-\varepsilon^{PBE}]$ between states 164 and 165 represents the GW correction to the PBE gap. The quasiparticle corrections $[\varepsilon^{GW}-\varepsilon^{PBE}]$ for occupied and empty states are approximately constant close to the gap. Indeed, the GW corrections to the occupied states from state 128 (1.5 eV below the HOMO at the GW level) to 164 (the HOMO) fall within the energy interval 1.32−1.54 eV; with one exception, all the corrections to the unoccupied orbitals up to state 234 fall within the interval 1.19−1.42 eV. At higher energy, starting approximately from state 235 (2.6 eV above the LUMO at the GW level), the values of $[\varepsilon^{GW} - \varepsilon^{PBE}]$ tend to decrease and even become negative in some cases. A similar, unphysical

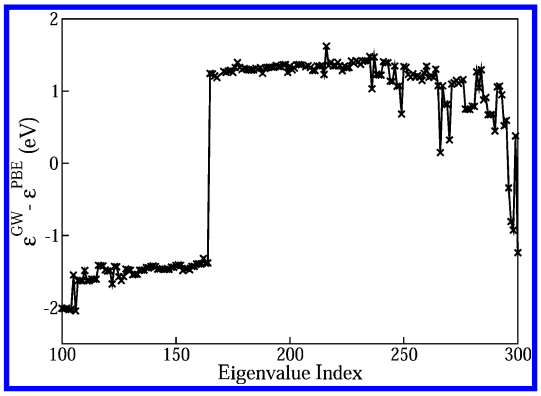

Figure 1. Difference between the computed quasiparticle energy ε^{GW} and the PBE eigenvalue ε^{PBE} for $Si_{66}H_{64}$ as a function of the eigenvalue index (see text). This system has 164 doubly occupied states. The energy width of the occupied states 100 to 164 is 3.21 eV; the energy interval between states 165 and 300 is 3.27 eV (at the GW level). These results were obtained with 840 eigenpotentials for the expansion of the dielectric matrix.

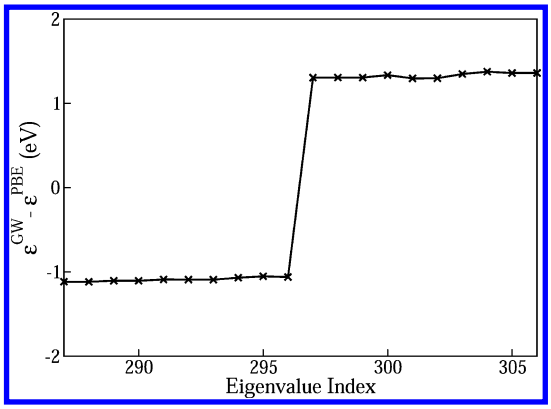

Figure 2. Difference between the computed quasiparticle energy ε^{GW} and the PBE eigenvalue ε^{PBE} for $Si_{124}H_{96}$ as a function of the eigenvalue index. This system has 296 doubly occupied states. The energy width of the occupied states 287 to 296 is 0.38 eV; the energy interval between states 297 and 306 is 0.50 eV (at the GW level). These results were obtained with 840 eigenpotentials for the expansion of the dielectric matrix.

behavior was also found in ref 36 for a $Si_{35}H_{36}$ nanoparticle (see Figure 6 of ref 36) for high-energy GW corrections. The magnitude of the GW corrections to high energy excitations most likely indicates a breakdown of the quasiparticle approximation, which is well justified in the case of states with long lifetimes and it is best fulfilled by electronic states near the HOMO and LUMO states.[54] We also note that the high energy unbound states are strongly affected by the boundary conditions and may not be accurately described in a finite-size supercell.

While these issues need further investigations, for the purpose of this work we choose a simple scissor operator for the BSE calculations. This approximation is reasonably accurate for the states close to the gap and circumvents the problems related to the quasiparticle corrections of high energy states. Furthermore, by using the scissor approximation (SA) the comparison of BSE and TDDFT results is straightforward, and it amounts to the effects of the different kernels used in the two formulations. The SA was also previously used in a similar study on smaller silicon nanoparticles by Benedict et al.[35]

The computed gap of $Si_{124}H_{96}$ (592 valence electrons) is 2.37 and 4.74 eV (obtained with 840 eigenpotentials) at the PBE and GW levels of theory, respectively. Figure 2 shows the difference $[\varepsilon^{GW}-\varepsilon^{PBE}]$ between the GW and PBE energy levels as a function of the eigenvalue index. In this case, since the system is much larger, it was possible to compute only few states at the GW level (from 287 to 306), corresponding to an energy interval of 5.6 eV. For the states close to the gap the behavior is analogous to that previously discussed for the $Si_{66}H_{64}$ nanoparticle and the use of the SA is a reasonable approximation also in this case. The validity of the SA for the large nanoparticles considered in this work is not a trivial consequence of the fact that this approximation is valid for bulk silicon.[5] Indeed, the $Si_{66}H_{64}$ and $Si_{124}H_{96}$ nanoparticles are both far from the bulk limit and exhibit strong quantum confinement effects: For example, their quasiparticle gaps are much larger than that of bulk silicon, which has a measured gap of 1.17 eV.[5] Furthermore, as shown in ref 55, the energy levels of silicon nanoparticles do not correspond simply to folded bands of bulk silicon.

The results for the optical absorption spectra of $Si_{66}H_{64}$ and $Si_{124}H_{96}$ are shown in Figure 3. Both systems will be discussed

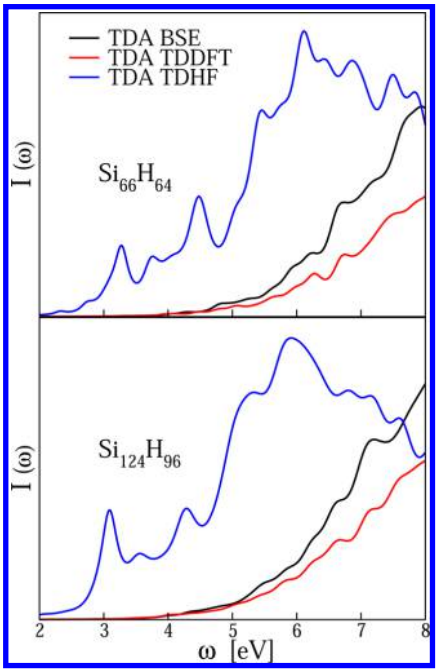

Figure 3. Absorption spectra of $Si_{66}H_{64}$ (top panel) and $Si_{124}H_{96}$ (bottom panel) computed at different levels of theory: Bethe–Salpeter equation (BSE), time-dependent density functional theory (TDDFT) using the adiabatic PBE approximation, and time-dependent Hartree–Fock (see text); TDA indicates the Tamm–Dancoff approximation. The TDDFT spectra have been arbitrarily blue-shifted by 0.1 eV in order to facilitate the comparison with the BSE results.

in parallel and we start with results obtained using the Tamm–Dancoff approximation (TDA).[56,57] The impact of this approximation will be explicitly discussed in the next section. Different levels of theory have been considered to compute the absorption spectra in Figure 3: The BSE, TDDFT in the adiabatic PBE approximation, and time-dependent Hartree–Fock (TDHF). Specifically, the TDHF spectra shown in Figure 3 are based on PBE orbitals and PBE energy levels corrected by the scissor shift derived from our GW calculations. While this is not a consistent way of performing TDHF calculations, the approximations used here allow for a straightforward

dx.doi.org/10.1021/ct5000956 | J. Chem. Theory Comput. 2014, 10, 3290–3298

comparison with BSE spectra, as TDHF and BSE results differ only by the effect of the screening present in the BSE kernel. In the BSE, the RPA screened Coulomb potential W is used in the kernel while in TDHF the bare Coulomb potential v is considered. As already well-known, for example, for bulk silicon, TDHF overestimates the binding energy of the excited electron to the corresponding hole,[58] leading to a redshift of the absorption threshold and a strong enhancement of the oscillator strength in the low energy part of the TDHF spectra. As expected for the Si nanoparticles studied here, the effect of the dielectric screening in the BSE kernel plays a key role in determining both the onset and intensity of the computed spectra. In Figure 3 we also compare BSE and TDDFT spectra, which were blue-shifted by 0.1 eV to facilitate the visual comparison. This small shift is comparable in magnitude to the numerical accuracy of our GW/BSE calculations. Although the peak intensities are different, it is interesting to see that the onset of the spectra and the main features in the low energy part of the TDDFT and BSE spectra are in good agreement (within 0.1−0.2 eV). The agreement in the onset of the TDDFT and BSE spectra is a nontrivial result, because for the BSE calculations we used a GW quasiparticle gap, while only uncorrected Kohn−Sham (KS) eigenvalues entered our TDDFT calculations. This finding indicates that a cancellation occurs, between the larger quasiparticle gap (instead of the KS HOMO−LUMO gap) and the exciton binding energy, as also discussed in previous works.[37,59] Our findings are in accord with previous suggestions presented in the literature, indicating that the difference between TDDFT and BSE spectra tends to be less pronounced for silicon nanoparticles with diameter larger than 1 nm (the largest nanoparticle considered in previous works was $Si_{47}H_{60}$).[35−37] However, it was yet to be shown that in the 1 to 2 nm size range these two methods yield results in agreement with each other, both for the absorption peak positions in the low energy part of the spectrum and for the absorption onset. Such an agreement is at variance with what found for other classes of systems, for which substantial differences were pointed out between BSE and TDDFT results; these systems include small hydrogenated Si clusters,[35−37] periodic solids,[15,26] periodic onedimensional nanostructures,[20] and molecular charge transfer excitations.[22,31]

Despite the good agreement of TDDFT and BSE results for peak positions and onset, the intensity of the spectra computed by these two methods is considerably different. The stronger oscillator strength of the BSE spectra at lower energy is very likely due to the stronger electron−hole interaction, as described by the BSE kernel. In TDHF, where the Coulomb interaction is not screened, the oscillator strength is strongly concentrated at lower energy. In BSE, the effect of the screening redistributes the oscillator strength at higher energy, but the low energy intensity still remains substantially larger than at the TDDFT level.

No experimental data are yet available on the hydrogenated Si clusters studied here. In previous studies, comparisons between theoretical and experimental results were presented only in the case of small hydrogenated silicon nanoclusters (SiH_4, Si_2H_6, Si_3H_8, and Si_5H_{12}) and for bulk silicon. For example, the experimental results for the absorption spectrum of silane SiH_4[60−63] appear to be well established and all in substantial agreement with each other; they show three very broad peaks associated with Rydberg transitions at 8.8, 9.7, and 10.7 eV. Some of the BSE and Monte Carlo calculations[37,64,65] found two peaks, with an intermediate transition possibly present with low intensity. The BSE calculations of refs 66 and 35 gave peak positions in fair agreement with experimental spectra (9.0, 10.2, and 11.2 eV; and 9.2, 9.9, and 11.4 eV, respectively) but the relative intensities of the transitions did not agree with those found experimentally. This disagreement may be partially due to the use of the TDA.[22] We also note that in the case of silane, it is very challenging to converge BSE calculations with respect to the number of empty states.[64] The TDDFT spectra of silane obtained with local and semilocal kernels are strongly red-shifted with respect to experiment (up to 1 eV for the transition at 10.7 eV).[67,68] The accuracy of local TDDFT for SiH_4 is significantly improved by using asymptotically correct potentials (the inaccuracy in the peak positions is at most 0.5 eV according to ref 28 and 0.2 eV according to ref 68).

The spectrum of disilane Si_2H_6 has been far less studied experimentally than that of silane.[60] Due to the more complex peak structure of both experimental and theoretical spectra, a comparison is less straightforward. Previous studies reported an accuracy for the peak positions within 0.6 eV for BSE[66] and within 0.4 eV for local TDDFT.[28,68] In ref 68, the TDDFT spectra of Si_3H_8 and Si_5H_{12} were compared to experiment, and the authors concluded that the use of asymptotically corrected functionals becomes less important as the size of the cluster is increased.

In ref 67, several hydrogenated silicon nanoparticles up to $Si_{147}H_{100}$ were studied at the TDLDA level and the computed gaps were extrapolated to be compared with experimental optical gaps of nanoparticles larger than 2 nm. Although this comparison is only qualitative and partially biased by the criterion used to define the gap (obtained by integrating the oscillator strength up to the value of 10^{-4}), the work of ref 67 suggests that TDLDA might give a reasonably accurate description of the experimental optical gaps of medium to large sized hydrogenated silicon nanoparticles, including the size range considered in our work.

We now turn to the discussion of sum rules and of the Tamm−Dancoff approximation (TDA).

4. TAMM−DANCOFF APPROXIMATION AND SUM RULES

To further understand the accuracy of BSE and TDDFT in predicting the intensity of absorption spectra, we carried out a numerical study of the Thomas−Reiche−Kuhn (f-sum) rule.[69−71] Since the f-sum rule is not satisfied within the TDA (see Appendix A), in this section we also consider TDDFT and BSE spectra computed without relying on this approximation. The comparison of TDDFT and BSE results without the TDA is analogous to the TDA case analyzed in section 3 and this discussion will not be repeated here. The effect of the TDA on the accuracy of BSE optical spectra of small molecules has been previously considered by several authors. In ref 21, it was shown that for azobenzene the TDA causes an error of about 0.2 eV in the peak position with respect to experiment. In ref 72, it was pointed out that the TDA may introduce an error as large as 0.4−0.5 eV with respect to the full BSE for biological chromophores. As discussed below, we find similar results for the spectra reported here. While a possible explanation for the failure of the TDA might reside in the mixed excitonic-plasmonic nature of excitations in molecules,[21] in this work we considered in detail only the effect of this approximation on the validity of sum rules.

The f-sum rule requires the integral of the absorption coefficient $I(\omega)$ between 0 and $+\infty$ to be proportional to the number of electrons N_e of the molecule (in atomic units):

$$f = \sum_{i=1}^{3} \int_0^{\infty} \omega[Im\alpha_{ii}(\omega)]d\omega = \frac{3}{2}N_e\pi \quad (1)$$

where α_{ii} indicates the diagonal components of the polarizability tensor. Equation 1 involves an integral between 0 and ∞ and of course it cannot help establish if the oscillator strength of a spectrum in a certain energy range is correctly described. However, the f-sum rule may help understand the accuracy in predicting the overall correct intensity of a spectrum. Our approach to solve the BSE and TDDFT equations is suitable to compute spectra in a large energy range and the f-sum rule can be verified in a straightforward way by integrating numerically eq 1.[51] Since our implementation uses pseudopotentials, in eq 1 N_e is equal to the number of valence electrons.

The BSE spectra obtained with and without the TDA are shown in Figure 4 for both $Si_{66}H_{64}$ (top panel) and $Si_{124}H_{96}$ (bottom panel). At low energy (insets of Figure 4) the main features of the spectra with and without TDA are similar, with differences in the peak positions always within 0.15 eV. However, particularly at high energy, the intensity of the two spectra is very different, with the TDA spectrum presenting a much stronger absorption. The exact same behavior has been found in the TDDFT spectra (not shown). These differences in the intensities have important implications on the f-sum rule.

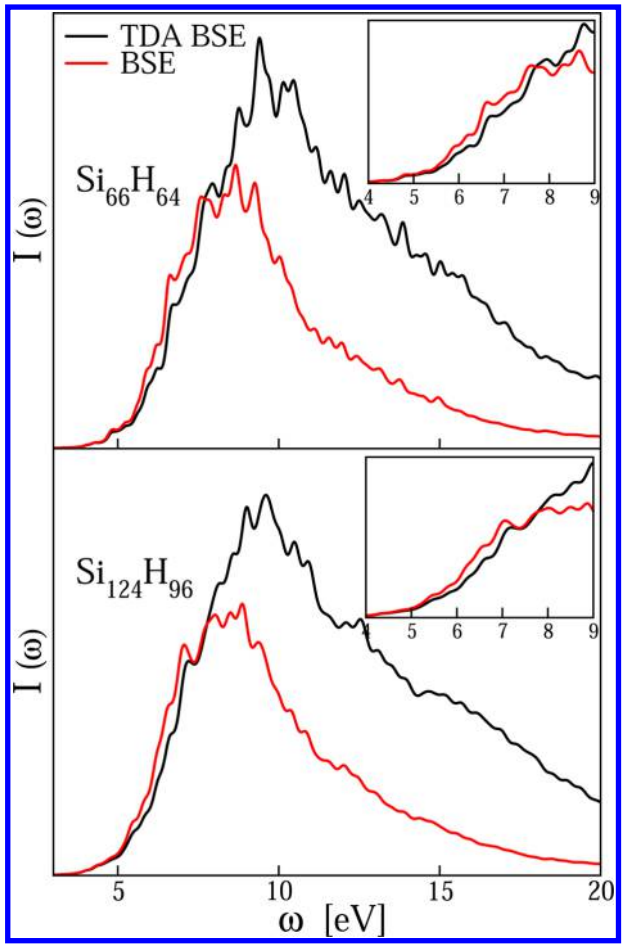

Figure 4. Comparison of the absorption spectrum for $Si_{66}H_{64}$ (top panel) and $Si_{124}H_{96}$ (bottom panel) computed by solving the Bethe–Salpeter equation with (TDA BSE) and without (BSE) the Tamm–Dancoff approximation. In the insets the spectra are shown in the 4–9 eV range.

The results for the f-sum rule are reported in Table 1 for both nanoparticles considered in this study. In the case of TDDFT spectra the f-sum rule is best satisfied, within 95%. The remaining error may stem from the nonlocal part of the pseudopotential (see Appendix A) or from the finite-size of the basis set.[51] Because the intensity of the TDA TDDFT spectrum at high energy is significantly stronger than the full TDDFT intensity (not shown, but similar to Figure 4 for BSE), the TDA TDDFT spectrum strongly overestimates the f-sum rule value. A discussion of the reason why the TDA fails to accurately fulfill the f-sum rule is given in Appendix A. At the BSE level, we found a more serious underestimation of the sum rule than at the TDDFT level (see Table 1) and a similar strong overestimation within the TDA. As discussed in Appendix A, this error of the BSE (even without TDA) is mainly due to the inconsistency between the GW or scissor approximation used for the quasiparticle energies and the approximation used in the kernel, which is based on the statically screened exchange self-energy. This inconsistency does not allow for an exact cancellation of the nonlocal terms in the ground state quasiparticle Hamiltonian and the kernel. The solution of this problem is certainly not trivial: The use of the statically screened approximation leads to rather inaccurate quasiparticle energies, while the inclusion of dynamical effects in the kernel[73,74] considerably increases the complexity of the method and its computational cost. However, it might be important to address this point in the future in order to obtain an improved description of the intensities of BSE spectra.

Table 1. Numerical Verification of the f-sum Rule for the $Si_{66}H_{64}$ and $Si_{124}H_{96}$ Nanoparticles at Different Levels of Theory: Time-Dependent Density Functional Theory (TDDFT) in the Adiabatic PBE Approximation[43] and Bethe–Salpeter Equation (BSE)[a]

nanoparticle	TDDFT	BSE	TDA-TDDFT	TDA-BSE
$Si_{66}H_{64}$	95.2%	80.9%	178.6%	162.3%
$Si1_{24}H_{96}$	95.0%	89.5%	180.7%	177.9%

[a]TDA Indicates the Tamm–Dancoff Approximation. The table reports the percentage corresponding to the ratio f^{num}/f^{exact} between the numerical value f^{num} obtained from the integral in eq 1 and the expected exact value f^{exact} that is proportional to the number of valence electrons N_e.

In a previous work[15] we showed numerically that the f-sum rule is well satisfied in the case of bulk silicon: 97% in the case of the full BSE and 107% in the case of TDA-BSE. However, the approximations often used in the numerical solution of the BSE (i.e., the TDA, the static approximation of the BSE kernel, the use of DFT orbitals as quasiparticle wave functions, and the scissor approximation) all work much better in the case of bulk silicon[12−15] than for molecular systems.[14,21,22,36]

5. CONCLUSIONS

In conclusion, we have applied recently developed many body perturbation theory methods[11,15,22,38,39] to study the excited states properties of silicon nanoparticles with diameters of 1.2 and 1.6 nm. The computed absorption spectra have been

compared with the results obtained at the TDDFT level of theory, showing that the position of the TDDFT and BSE absorption peaks are in good agreement (within 0.1−0.2 eV). Our findings point at the following, qualitative conclusion: There is a size regime, for diameter larger than ≈1.2 nm and presumably smaller than 4−5 nm, where the exciton binding energy (e_b) of the NPs and the GW corrections (Δ_{GW}) to Kohn−Sham gaps cancel each other. Hence, numerically the HOMO−LUMO Kohn−Sham gap is a good approximation of the optical gap of the nanoparticles. The cancellation of the terms e_b and Δ_{GW} is responsible for yielding the same onset of the TDDFT and BSE spectra (within 0.1−0.2 eV). Since the GW corrections close to the gap are approximately constant as a function of energy and presumably so also the exciton binding, the positions of the TDDFT and BSE peaks turn out to be similar. However, the intensities of the TDDFT and BSE spectra differ through the whole energy range.

We have also conducted a numerical study of the f-sum rule for all computed spectra. In the BSE case the f-sum rule is not fully satisfied, even in the absence of the Tamm−Dancoff approximation. Work is in progress to further investigate this issue, so as to better understand the accuracy of the BSE for molecules and zero dimensional nanostructures.

APPENDIX A

Thomas−Reiche−Kuhn Sum Rule in the Bethe−Salpeter Equation

In this appendix, we discuss in detail the validity of the Thomas−Reiche−Kuhn (f-sum)[69−71] rule for the BSE. Atomic units ($\hbar = m = e = 1$) will be used throughout this appendix. In the general Green's function framework the validity of the f-sum rule is discussed in terms of conserving approximations.[4] The analysis below is meant to be specifically valid for the BSE with approximations typically used within the computational materials science community, that is, statically screened exchange term in the kernel and quasiparticle corrections within the GW approximation (or, as in this paper, using a scissor operator).[10,11] We will use the density matrix perturbation theory formalism of ref 22, but the conclusions are valid also for the electron−hole implementation.[12−14] While the validity of the f-sum rule is well demonstrated for local TDDFT[8,51,75] and TDHF,[76,77] we investigate here if eq 1 holds when the polarizability α is approximated at the BSE level of theory. The formalism derived in ref 22 is equivalent to a time-dependent Coulomb-hole plus screened-exchange (TDCOHSEX). The kernel of the TDCOHSEX is equivalent to the kernel of the BSE. However, since the COHSEX approximation strongly overestimates quasiparticle gaps, the GW quasiparticle energies are used instead. Here, we will first demonstrate the validity of the f-sum rule for the TDCOHSEX starting from a fully self-consistent COHSEX ground-state. In this case, the f-sum rule eq 1 is satisfied because of the cancellation of the non-local terms coming from the kernel and the quasiparticle Hamiltonian. Since the BSE uses the GW approximation to describe quasiparticle energies, the "inconsistency" between the kernel and the quasiparticle Hamiltonian makes an exact cancellation impossible.

In the following, for the sake of simplicity, we will consider all the eigenstates of the Hamiltonian as real (they can always be chosen to be real for molecular systems in the presence of time-reversal symmetry). Following ref 22, the xx component of the TDCOHSEX (or BSE) polarizability can be expressed as

$$\alpha_{xx}(\omega) = -\langle(\mathbf{a},\mathbf{a})|(\omega - \mathcal{L} + i\eta)^{-1}|(\mathbf{a},-\mathbf{a})\rangle \tag{2}$$

where η is a positive infinitesimal, the Liouvillian operator $\mathcal{L}$ is defined as

$$\mathcal{L} = \begin{pmatrix} \mathcal{D} + 2\mathcal{K}^x - \mathcal{K}^{1d} & 2\mathcal{K}^x - \mathcal{K}^{2d} \\ -2\mathcal{K}^x + \mathcal{K}^{2d} & -\mathcal{D} - 2\mathcal{K}^x + \mathcal{K}^{1d} \end{pmatrix} \tag{3}$$

and the vector

$$\mathbf{a} = \begin{pmatrix} |a_1\rangle \\ \vdots \\ |a_N\rangle \end{pmatrix} = \begin{pmatrix} \hat{Q}x|\phi_1\rangle \\ \vdots \\ \hat{Q}x|\phi_N\rangle \end{pmatrix} \tag{4}$$

is the batch of the orbitals $|a\rangle = \hat{Q}x|\phi\rangle$ representing the position operator x; $\hat{Q}$ is the projector onto the unoccupied state subspace, N the number of occupied states, and ϕ indicates the quasiparticle orbitals at the self-consistent COHSEX level of theory. The batch vector $\mathbf{a}$ in eq 4 contains N orbitals and the vectors $(\mathbf{a},\mathbf{a})$ and $(\mathbf{a},-\mathbf{a})$ contain 2N orbitals. The polarizability in eq 2 is the explicit batch representation[48] of the polarizability in eq 6 of ref 22. The application of $\mathcal{D}$, $\mathcal{K}^x$, $\mathcal{K}^{1d}$, and $\mathcal{K}^{2d}$ in eq 3 to the batch vector $\mathbf{a}$ is defined as

$$\mathcal{D}_{v,v'}|a_{v'}\rangle = (\hat{H} - \varepsilon_{v'})\delta_{vv'}|a_{v'}\rangle \tag{5}$$

$$\mathcal{K}^x_{v,v'}|a_{v'}\rangle = \hat{Q}\left(\int \frac{1}{|\mathbf{r}-\mathbf{r}'|}\phi_{v'}(\mathbf{r}')a_{v'}(\mathbf{r}')\mathrm{d}\mathbf{r}'\right)|\phi_v\rangle \tag{6}$$

$$\mathcal{K}^{1d}_{v,v'}|a_{v'}\rangle = \hat{Q}\left(\int W(\mathbf{r},\mathbf{r}')\phi_{v'}(\mathbf{r}')\phi_v(\mathbf{r}')\mathrm{d}\mathbf{r}'\right)|a_{v'}\rangle \tag{7}$$

$$\mathcal{K}^{2d}_{v,v'}|a_{v'}\rangle = \hat{Q}\left(\int W(\mathbf{r},\mathbf{r}')a_{v'}(\mathbf{r}')\phi_v(\mathbf{r}')\mathrm{d}\mathbf{r}'\right)|\phi_{v'}\rangle \tag{8}$$

where the subscripts v and v' run from 1 to N, $\hat{H}$ is the quasiparticle COHSEX Hamiltonian, and W indicates the screened Coulomb potential. Usually explicit GW corrections are used instead of the COHSEX Hamiltonian.[10,12,14]

The operator $\mathcal{L}$ is non-Hermitian, but the corresponding left and right eigenvectors correspond to a biorthogonal complete set of vectors.[76,77] We define the right and left eigenvectors as $(\mathbf{p}_n,\mathbf{q}_n)$ and $(\mathbf{p}_n,-\mathbf{q}_n)$, respectively, and the corresponding positive eigenvalue (TDCOHSEX or BSE excitation energy) as E_n. Because of the structure of $\mathcal{L}$ in eq 3, we have that for each positive eigenvalue E_n there is a corresponding negative eigenvalue $-E_n$, with right eigenvector $(\mathbf{q}_n,\mathbf{p}_n)$ and left eigenvector $(\mathbf{q}_n,-\mathbf{p}_n)$. Since only the positive eigenvalues $E_n > 0$ contribute to the integral in eq 1, we have

$$\begin{aligned} &\int_0^\infty \omega[Im\alpha_{xx}(\omega)]\mathrm{d}\omega \\ &= \pi \sum_n^{(E_n>0)} \int_0^\infty \omega[\langle(\mathbf{a},\mathbf{a})|(\mathbf{p}_n,\mathbf{q}_n)\rangle\langle(\mathbf{p}_n,-\mathbf{q}_n)|(\mathbf{a},-\mathbf{a})\rangle \\ &\quad \times \delta(\omega - E_n)]\mathrm{d}\omega \\ &= \pi \sum_n^{(E_n>0)} E_n\langle(\mathbf{a},\mathbf{a})|(\mathbf{p}_n,\mathbf{q}_n)\rangle\langle(\mathbf{p}_n,-\mathbf{q}_n)|(\mathbf{a},-\mathbf{a})\rangle \\ &= \frac{\pi}{2}\langle(\mathbf{a},\mathbf{a})|\mathcal{L}\cdot|(\mathbf{a},-\mathbf{a})\rangle \end{aligned} \tag{9}$$

dx.doi.org/10.1021/ct5000956 | J. Chem. Theory Comput. 2014, 10, 3290−3298

From the definition of $\mathcal{L}$ in eq 3, the matrix element in eq 9 takes the form:

$$\frac{1}{2}\langle(\mathbf{a},\mathbf{a})|\mathcal{L}\cdot|(\mathbf{a},-\mathbf{a})\rangle = \langle\mathbf{a}|\mathcal{D}|\mathbf{a}\rangle - \langle\mathbf{a}|\mathcal{K}^{1d}|\mathbf{a}\rangle + \langle\mathbf{a}|\mathcal{K}^{2d}|\mathbf{a}\rangle \tag{10}$$

where the first term at the second member of the equation can be expressed as

$$\langle\mathbf{a}|\mathcal{D}|\mathbf{a}\rangle = \sum_{v} \langle\phi_v|x\hat{Q}(\hat{H}-\varepsilon_v)\hat{Q}x|\phi_v\rangle \tag{11}$$

$$= \sum_{v,c} \langle\phi_v|x|\phi_c\rangle\langle\phi_c|x|\phi_v\rangle(\varepsilon_c-\varepsilon_v) \tag{12}$$

$$= \sum_{v,c} \langle\phi_v|x|\phi_c\rangle\langle\phi_c|[\hat{H},x]|\phi_v\rangle \tag{13}$$

the subscript c in eqs 12 and 13 indicates conduction (empty) states.

We can write the ground-state COHSEX Hamiltonian as

$$\hat{H} = \hat{H}_{\mathrm{loc}} + \Sigma_{\mathrm{SEX}} = \hat{H}_{\mathrm{loc}} - \sum_{v} W(\mathbf{r},\mathbf{r}')\phi_v(\mathbf{r})\phi_v(\mathbf{r}') \tag{14}$$

where we have separated the local contributions to the Hamiltonian $\hat{H}_{\mathrm{loc}}$ (including the COH self-energy) from the non-local Σ_{SEX} self-energy. Since in this work we use non-local pseudopotentials, additional non-local terms should be explicitly considered in eq 14. For the sake of simplicity we will not discuss the contribution of these terms that, however, influence the validity of the sum rule both in BSE and TDDFT.[51] We will start by considering the non-local contribution of $\hat{H}$ (eq 14) to the commutators in eq 13:

$$\sum_{v,c} \langle\phi_v|x|\phi_c\rangle\langle\phi_c|[\Sigma_{\mathrm{SEX}},x]|\phi_v\rangle = \langle\mathbf{a}|\mathcal{K}^{1d}|\mathbf{a}\rangle - \langle\mathbf{a}|\mathcal{K}^{2d}|\mathbf{a}\rangle \tag{15}$$

In order to derive the result in eq 15, it is easy to notice that $\langle\phi_v|x|\phi_c\rangle\langle\phi_c| = \langle\phi_v|x\hat{Q} = \langle a_v|$ (see eq 4) and to substitute the explicit definition of Σ_{SEX} (eq 14):

$$\sum_{v,c} \langle\phi_v|x|\phi_c\rangle\langle\phi_c|[\Sigma_{\mathrm{SEX}},x]|\phi_v\rangle = \sum_{v,v'} \int a_v(\mathbf{r})x\phi_{v'}(\mathbf{r})W(\mathbf{r},\mathbf{r}')\phi_{v'}(\mathbf{r}')\phi_v(\mathbf{r}')\mathrm{d}\mathbf{r}\mathrm{d}\mathbf{r}' - \sum_{v,v'} \int a_v(\mathbf{r})\phi_{v'}(\mathbf{r})W(\mathbf{r},\mathbf{r}')\phi_{v'}(\mathbf{r}')x'\phi_v(\mathbf{r}')\mathrm{d}\mathbf{r}\mathrm{d}\mathbf{r}' \tag{16}$$

We can then consider the expansion $x\phi_{v'}(\mathbf{r}) = \Sigma_i\phi_i(\mathbf{r})\int\phi_i(\mathbf{r}')x\phi_{v'}(\mathbf{r}')\mathrm{d}\mathbf{r}'$ (where the sum is over all the states, that constitute a complete basis set); it can be shown that the contributions of the occupied ϕ_i's cancel between the two terms at the second member of eq 16 and only the projection on the unoccupied states $\Sigma_c\phi_c(\mathbf{r})\int\phi_c(\mathbf{r}')x\phi_{v'}(\mathbf{r}')\mathrm{d}\mathbf{r}' = a_{v'}(\mathbf{r})$ contributes to the expansion of $x\phi_{v'}(\mathbf{r})$ in eq 16. Remembering the definitions in eqs 7 and 8, this leads to the result in eq 15. According to eq 15, the non-local contribution to the quasiparticle Hamiltonian (eq 15) exactly compensates the contributions from the kernel (last two terms in eq 10). In eq 10, the only remaining component comes from the local part of the Hamiltonian:

$$\sum_{v,c} \langle\phi_v|x|\phi_c\rangle\langle\phi_c|[\hat{H}_{\mathrm{loc}},x]|\phi_v\rangle = \frac{1}{2}\sum_{v,c}[\langle\phi_v|x|\phi_c\rangle\langle\phi_c|[\hat{H}_{loc},x]|\phi_v\rangle - \langle\phi_v|[\hat{H}_{\mathrm{loc}},x]|\phi_c\rangle\langle\phi_c|x|\phi_v\rangle] = \frac{1}{2i}\sum_{v,c}[\langle\phi_v|x|\phi_c\rangle\langle\phi_c|p_x|\phi_v\rangle - \langle\phi_v|p_x|\phi_c\rangle\langle\phi_c|x|\phi_v\rangle] = \frac{1}{2i}\sum_{v}\langle\phi_v|[x,p_x]|\phi_v\rangle = \frac{1}{2}N_e \tag{17}$$

where we took advantage of $[\hat{H}_{\mathrm{loc}},x]$ being proportional to the momentum operator p_x and $[x,p_x]$ being a constant. Since eq 15 exactly cancels the last two terms in eq 10, eq 17 gives the only non-zero contribution to eq 10, namely $\langle(\mathbf{a},\mathbf{a})|\mathcal{L}\cdot|(\mathbf{a},-\mathbf{a})\rangle/2 = N_e/2$. From this result, by including a factor π that comes from eq 9 and a factor 3 that comes from the sum over the Cartesian components, the f-sum rule in eq 1 is derived.

This derivation is valid for TDCOHSEX based on a fully self-consistent ground state. Although the TDCOHSEX equations are similar to the BSE, the generalization to the BSE of the demonstration presented in this section requires particular care for two main reasons:

- In order to numerically solve the BSE, the quasiparticle orbitals are approximated by self-consistent DFT orbitals ϕ_i^{DFT}. Accordingly, these orbitals are not eigenstates of any quasiparticle Hamiltonian $\hat{H}$ and eq 13 cannot be derived from eq 12 (or, similarly, eq 12 cannot be derived from eq 11). In practice GW energy levels are usually computed perturbatively starting from DFT states, within the so-called G_0W_0 approach. A GW Hamiltonian can then be defined as $\hat{H}^{\mathrm{GW}} = \Sigma_i\varepsilon_i^{\mathrm{GW}}|\phi_i^{\mathrm{DFT}}\rangle\langle\phi_i^{\mathrm{DFT}}|$. By using such Hamiltonian, eq 13 may still be derived from eq 12. In the present work we have used a scissor operator. Within this approximation the orbitals ϕ_i^{DFT} are still eigenstates of the Hamiltonian and the set of eqs 11−13 is still valid.
- If the GW or a scissor operator are used to approximate the quasiparticle Hamiltonian (or, equivalently, the quasiparticle energies), $\hat{H}$ in eq 14 does not contain Σ_{SEX} and the cancellation between eq 15 and the last two terms in eq 10 may not be obtained. This problem cannot be easily overcome and affects all practical BSE implementations.

This discussion shows that in order to rigorously satisfy the f-sum rule an approximation to the BSE kernel should be used which is consistent with that adopted for the quasiparticle energies, in order to consistently cancel non-local contributions. Indeed, the BSE spectra computed in this work exhibit a less satisfactory verification of the f-sum rule than our TDDFT results.

As shown in section 4, the TDA leads to a significant overestimation of the f-sum rule up to 70-80% for both TDDFT and BSE. Within this approximation the two off-diagonal blocks ($2\mathcal{K}^x - \mathcal{K}^{2d}$ and $-2\mathcal{K}^x + \mathcal{K}^{2d}$) in eq 3 are discarded. Within the TDA the matrix element in eq 10 takes the form

$$\frac{1}{2}\langle\mathbf{a}|\mathcal{L}^{\mathrm{TDA}}|\mathbf{a}\rangle = \langle\mathbf{a}|\mathcal{D}|\mathbf{a}\rangle + 2\langle\mathbf{a}|\mathcal{K}^{x}|\mathbf{a}\rangle - \langle\mathbf{a}|\mathcal{K}^{1d}|\mathbf{a}\rangle \tag{18}$$

dx.doi.org/10.1021/ct5000956 | J. Chem. Theory Comput. 2014, 10, 3290−3298

and the demonstration presented in this appendix does not apply. This explains the numerical results of section 4 for the TDA.

AUTHOR INFORMATION

Corresponding Author

*Email: dario.rocca@univ-lorraine.fr.

Notes

The authors declare no competing financial interest.

ACKNOWLEDGMENTS

Part of this work was supported by DOE/BSE grant DE-FG02-06ER46262 and by NSF Solar Collaborative DMR-1035468. A.G. acknowledges the support of the Lendület program from the Hungarian Academy of Sciences. Computer time was provided by Grand Equipement National de Calcul Intensif via the project x2013085106 and NIIF supercomputing center in Debrecen, Hungary.

REFERENCES

(1) Hedin, L. *Phys. Rev.* **1965**, *139*, A796−A823.
(2) Hanke, W.; Sham, L. *Phys. Rev. B* **1980**, *21*, 4656.
(3) Strinati, G. *Phys. Rev. B* **1984**, *29*, 5718.
(4) Strinati, G. *La Rivista del Nuovo Cimento* **1988**, *11*, 1−86.
(5) Hybertsen, M. S.; Louie, S. G. *Phys. Rev. B* **1986**, *34*, 5390−5413.
(6) Godby, R. W.; Schlüter, M.; Sham, L. J. *Phys. Rev. B* **1988**, *37*, 10159−10175.
(7) Runge, E.; Gross, E. K. *Phys. Rev. Lett.* **1984**, *52*, 997.
(8) Casida, M. E. *Recent Advances in Density Functional Methods, Part I*; World Scientific: Singapore, 1995; p 155.
(9) Bauernschmitt, R.; Ahlrichs, R. *Chem. Phys. Lett.* **1996**, *256*, 454−464.
(10) Onida, G.; Reining, L.; Rubio, A. *Rev. Mod. Phys.* **2002**, *74*, 601−659.
(11) Ping, Y.; Rocca, D.; Galli, G. *Chem. Soc. Rev.* **2013**, *42*, 2437−2469.
(12) Albrecht, S.; Reining, L.; Del Sole, R.; Onida, G. *Phys. Rev. Lett.* **1998**, *80*, 4510−4513.
(13) Benedict, L. X.; Shirley, E. L.; Bohn, R. B. *Phys. Rev. Lett.* **1998**, *80*, 4514−4517.
(14) Rohlfing, M.; Louie, S. G. *Phys. Rev. B* **2000**, *62*, 4927−4944.
(15) Rocca, D.; Ping, Y.; Gebauer, R.; Galli, G. *Phys. Rev. B* **2012**, *85*, 045116.
(16) Ping, Y.; Rocca, D.; Galli, G. *Phys. Rev. B* **2013**, *87*, 165203.
(17) Spataru, C. D.; Ismail-Beigi, S.; Benedict, L. X.; Louie, S. G. *Phys. Rev. Lett.* **2004**, *92*, 077402.
(18) Wirtz, L.; Marini, A.; Rubio, A. *Phys. Rev. Lett.* **2006**, *96*, 126104.
(19) Bruno, M.; Palummo, M.; Marini, A.; Del Sole, R.; Ossicini, S. *Phys. Rev. Lett.* **2007**, *98*, 036807.
(20) Ping, Y.; Rocca, D.; Lu, D.; Galli, G. *Phys. Rev. B* **2012**, *85*, 035316.
(21) Gruning, M.; Marini, A.; Gonze, X. *Nano Lett.* **2009**, *9*, 2820−2824.
(22) Rocca, D.; Lu, D.; Galli, G. *J. Chem. Phys.* **2010**, *133*, 164109.
(23) Casida, M. E.; Jamorski, C.; Casida, K. C.; Salahub, D. R. *J. Chem. Phys.* **1998**, *108*, 4439−4449.
(24) Stratmann, R. E.; Scuseria, G. E.; Frisch, M. J. *J. Chem. Phys.* **1998**, *109*, 8218−8224.
(25) Rocca, D.; Bai, Z.; Li, R.-C.; Galli, G. *J. Chem. Phys.* **2012**, *136*, 034111.
(26) Reining, L.; Olevano, V.; Rubio, A.; Onida, G. *Phys. Rev. Lett.* **2002**, *88*, 066404.
(27) Tozer, D. J.; Amos, R. D.; Handy, N. C.; Roos, B. O.; Serrano-Andres, L. *Mol. Phys.* **1999**, *97*, 859−868.
(28) Marques, M.; Castro, A.; Rubio, A. *J. Chem. Phys.* **2001**, *115*, 3006−3014.
(29) Dreuw, A.; Weisman, J. L.; Head-Gordon, M. *J. Chem. Phys.* **2003**, *119*, 2943−2946.
(30) Peach, M. J. G.; Benfield, P.; Helgaker, T.; Tozer, D. J. *J. Chem. Phys.* **2008**, *128*, 044118.
(31) Blase, X.; Attaccalite, C. *Appl. Phys. Lett.* **2011**, *99*, 171909.
(32) Stein, T.; Kronik, L.; Baer, R. *J. Am. Chem. Soc.* **2009**, *131*, 2818−2820.
(33) Sottile, F.; Olevano, V.; Reining, L. *Phys. Rev. Lett.* **2003**, *91*, 056402.
(34) Marini, A.; Del Sole, R.; Rubio, A. *Phys. Rev. Lett.* **2003**, *91*, 256402.
(35) Benedict, L. X.; Puzder, A.; Williamson, A. J.; Grossman, J. C.; Galli, G.; Klepeis, J. E.; Raty, J.-Y.; Pankratov, O. *Phys. Rev. B* **2003**, *68*, 085310.
(36) Tiago, M. L.; Chelikowsky, J. R. *Phys. Rev. B* **2006**, *73*, 205334.
(37) Ramos, L. E.; Paier, J.; Kresse, G.; Bechstedt, F. *Phys. Rev. B* **2008**, *78*, 195423.
(38) Nguyen, H.-V.; Pham, T. A.; Rocca, D.; Galli, G. *Phys. Rev. B* **2012**, *85*, 081101.
(39) Pham, T. A.; Nguyen, H.-V.; Rocca, D.; Galli, G. *Phys. Rev. B* **2013**, *87*, 155148.
(40) The GW calculations for $Si_{124}H_{96}$ took about one week on 120 Intel Xeon X5680 processors of a machine with 12 processors and 4 GB memory per node; the Bethe−Salpeter calculation took approximately 8 weeks on the same machine with the same number of processors. A direct comparison of the performance of our code with previous (electron−hole) implementations is not straightforward. Indeed, the algorithms used in this work include automatically all the empty states described by the plane-wave basis set (more than 320 000 for $Si_{124}H_{96}$) and use the full kinetic energy cutoff to represent the dielectric matrix. This level of convergence would be hard (most likely impossible) to reach within a traditional implementation, but it is important, for example, to verify numerically the f-sum rule.
(41) Tilley, R. D.; Warner, J. H.; Yamamoto, K.; Matsui, I.; Fujimori, H. *Chem. Commun.* **2005**, 1833−1835.
(42) Rosso-Vasic, M.; Spruijt, E.; van Lagen, B.; De Cola, L.; Zuilhof, H. *Small* **2008**, *4*, 1835−1841.
(43) Perdew, J. P.; Burke, K.; Ernzerhof, M. *Phys. Rev. Lett.* **1996**, *77*, 3865−3868.
(44) Giannozzi, P.; et al. *J. Phys.: Condens. Matter* **2009**, *21*, 5502.
(45) Wilson, H. F.; Gygi, F.; Galli, G. *Phys. Rev. B* **2008**, *78*, 113303.
(46) Nguyen, H.-V.; de Gironcoli, S. *Phys. Rev. B* **2009**, *79*, 205114.
(47) Baroni, S.; de Gironcoli, S.; Dal Corso, A.; Giannozzi, P. *Rev. Mod. Phys.* **2001**, *73*, 515−562.
(48) Rocca, D.; Gebauer, R.; Saad, Y.; Baroni, S. *J. Chem. Phys.* **2008**, *128*, 154105.
(49) Umari, P.; Stenuit, G.; Baroni, S. *Phys. Rev. B* **2010**, *81*, 115104.
(50) Walker, B.; Saitta, A. M.; Gebauer, R.; Baroni, S. *Phys. Rev. Lett.* **2006**, *96*, 113001.
(51) Malcioğlu, O. B.; Gebauer, R.; Rocca, D.; Baroni, S. *Comput. Phys. Commun.* **2011**, *182*, 1744−1754.
(52) Rocca, D. *J. Chem. Phys.* **2014**, *140*, 18A501.
(53) For the states 169−170 we obtained unphysically large GW corrections. Because these values are likely due to numerical instabilities, they are not included in Figure 1 and in the discussion of this paper. A possible explanation of this behavior might be related to the use of the analytic continuation approach and could be overcome by implementing the contour integral method.[58]
(54) Hedin, L.; Lundqvist, S. *Solid State Phys.* **1970**, *23*, 1−181.
(55) Kocevski, V.; Eriksson, O.; Rusz, J. *Phys. Rev. B* **2013**, *87*, 245401.
(56) Tamm, I. *J. Phys. (Moscow)* **1945**, *78*, 382.
(57) Dancoff, S. M. *Phys. Rev.* **1950**, *78*, 382−385.
(58) Bruneval, F. Exchange and correlation in the Electronic Structure of Solids, from Silicon to Cuprous Oxide: GW Approximation and Beyond. PhD Thesis, École Polytechnique, Palaiseau, France, 2006; available online: http://theory.polytechnique.fr/people/bruneval/fabien.html.

(59) Delerue, C.; Lannoo, M.; Allan, G. *Phys. Rev. Lett.* **2000**, *84*, 2457.
(60) Itoh, U.; Toyoshima, Y.; Onuki, H.; Washida, N.; Ibuki, T. *J. Chem. Phys.* **1986**, *85*, 4867−4872.
(61) Kameta, K.; Ukai, M.; Terazawa, N.; Nagano, K.; Chikahiro, Y.; Kouchi, N.; Hatano, Y.; Tanaka, K. *J. Chem. Phys.* **1991**, *95*, 6188−6189.
(62) Wu, C. Y. R.; Chen, F. Z.; Judge, D. L. *J. Chem. Phys.* **1993**, *99*, 1530−1536.
(63) Cooper, G.; Burton, G. R.; Chan, W. F.; Brion, C. E. *Chem. Phys.* **1995**, *196*, 293−306.
(64) Hahn, P. H.; Schmidt, W. G.; Bechstedt, F. *Phys. Rev. B* **2005**, *72*, 245425.
(65) Porter, A. R.; Al-Mushadani, O. K.; Towler, M. D.; Needs, R. J. *J. Chem. Phys.* **2001**, *114*, 7795−7804.
(66) Rohlfing, M.; Louie, S. G. *Phys. Rev. Lett.* **1998**, *80*, 3320−3323.
(67) Vasiliev, I.; Öğüt, S.; Chelikowsky, J. R. *Phys. Rev. Lett.* **2001**, *86*, 1813.
(68) Vasiliev, I. *Phys. Status Solidi B* **2003**, *239*, 19−25.
(69) Thomas, W. *Naturwissenschaften* **1925**, *13*, 627.
(70) Kuhn, W. *Z. Phys.* **1925**, *33*, 408.
(71) Reiche, F.; Thomas, W. *Z. Phys.* **1925**, *34*, 510.
(72) Ma, Y.; Rohlfing, M.; Molteni, C. *Phys. Rev. B* **2009**, *80*, 241405.
(73) Bechstedt, F.; Tenelsen, K.; Adolph, B.; Del Sole, R. *Phys. Rev. Lett.* **1997**, *78*, 1528.
(74) Marini, A.; Del Sole, R. *Phys. Rev. Lett.* **2003**, *91*, 176402.
(75) Jamorski, C.; Casida, M. E.; Salahub, D. R. *J. Chem. Phys.* **1996**, *104*, 5134−5147.
(76) Thouless, D. *Nucl. Phys.* **1961**, *22*, 78−95.
(77) McLachlan, A. D.; Ball, M. A. *Rev. Mod. Phys.* **1964**, *36*, 844−855.